CARBON 49 (2011) 4111–4121

available at www.sciencedirect.com

ScienceDirect

journal homepage: www.elsevier.com/locate/carbon

Mechanical properties of graphyne

Steven W. Cranford [a,b], *Markus J. Buehler* [a,b,*]

[a] *Center for Materials Science and Engineering, Massachusetts Institute of Technology, 77 Massachusetts Ave., Cambridge, MA, USA*
[b] *Laboratory for Atomistic and Molecular Mechanics, Department of Civil and Environmental Engineering, Massachusetts Institute of Technology, 77 Massachusetts Ave., Room 1-235A&B, Cambridge, MA, USA*

ARTICLE INFO

Article history:
Received 22 March 2011
Accepted 18 May 2011
Available online 23 May 2011

ABSTRACT

Carbon nanotubes and graphene have paved the way for the next step in the evolution of carbon materials. Among the novel forms of carbon allotropes is graphyne – a two-dimensional lattice of sp–sp^2-hybridized carbon atoms similar to graphene for which recent progress has been made in synthesizing dehydrobenzoannulene precursors that form subunits of graphyne. Here, we characterize the mechanical properties of single-atomic-layer graphyne sheets by full atomistic first-principles-based ReaxFF molecular dynamics. Atomistic modeling is carried out to determine its mechanical properties for both in-plane and bending deformation including material failure, as well as intersheet adhesion. Unlike graphene, the fracture strain and stress of graphyne depends strongly on the direction of the applied strain and the alignment with carbon triple-bond linkages, ranging from 48.2 to 107.5 GPa with ultimate strains of 8.2–13.2%. The intersheet adhesion and out-of-plane bending stiffnesses are comparable to graphene, despite the density of graphyne being only one-half of that of graphene. Unlike graphene, the sparser carbon arrangement in graphyne combined with the directional dependence on the acetylenic groups results in internal stiffening dependent on the direction of applied loading, leading to a nonlinear stress–strain behavior.

1. Introduction

The superlative properties and potential applications of synthetic carbon materials – particularly fullerenes [1], nanotubes [2] and graphene [3] – illustrate their unique scientific and technological importance and have motivated substantial research efforts in recent years. Recent investigations of "exotic" carbon allotropes – including the successful synthesis of carbyne [4] and graphdiyne [5], and the prediction of T-carbon [6,7] – illustrate the continuing interest in all-carbon chemistries beyond already known (and well studied) allotropes such as fullerenes, nanotubes, and graphene [8]. Among the remaining predicted forms of carbon allotropes [9], graphyne has been the subject of little yet continuing interest among structural, theoretical, and synthetic scientists due to its unknown electronic, optical, and mechanical properties [10–15], as well as proposed practical strategies of synthesis [14,16–18]. Although currently, large homogenous sheets of graphyne with long-range ordered (periodic) internal structures have not yet been reported, there are increasing efforts in the synthesis and assembly of a class of molecules known as dehydrobenzoannulenes (DBAs), a precursor and subunit of graphyne [14,18]. Indeed, new synthetic methods in annulene chemistry [19,20] now enable the assembly of a diverse array of DBA topologies, leading to an increasing potential and inevitable synthesis of graphyne. For example, recently the first successful synthesis of thin films of graphdiyne was achieved on copper substrates via a

* Corresponding author at: Department of Civil and Environmental Engineering, Massachusetts Institute of Technology, 77 Massachusetts Ave., Cambridge, MA, USA. Fax: +1 617 452 2750.
E-mail address: mbuehler@MIT.EDU (M.J. Buehler).
0008-6223/$ - see front matter © 2011 Elsevier Ltd. All rights reserved.
doi:10.1016/j.carbon.2011.05.024

cross-coupling reaction using hexaethynylbenzene [5]. There has been particular interest in terms of electronic properties, motivating previous theoretical, experimental and quantum-scale studies [13,21–23]. However, the elastic and mechanical properties, critical to successful implementation, have yet to be explicitly determined. In addition, the search for new modifications of carbon has produced several new classes of macrocycles that feature conjugated all-carbon backbones without annellated benzene rings and display highly interesting properties [24]. These systems – including dehydroannulenes, expanded radialenes, radiaannulenes, expanded "Platonic" objects, and alleno-acetylenic macrocycles – may well serve as precursors to graphyne in the near future [24]. In the interim, the mechanical characterization approach outlined herein can equally be applied to such molecular substructures to exploit the combinatorial features of mixed carbon networks (such as unique molecular architectures based on expanded dehydroannulenes and expanded radialenes scaffolds).

The atomistic-level characterization techniques described herein are equally applicable to small, graphyne-like DBA substructures and can be immediately applied to various possible carbon geometries. To provide immediate quantitative comparison, there is an extensive catalogue of work currently available regarding the mechanics of carbon nanotubes and graphene facilitating a direct assessment of the mechanical performance of graphyne.

Naturally occurring carbon exists in only two allotropes, diamond and graphite, which consist of extended networks of sp^3- and sp^2-hybridized carbon atoms, respectively. Other ways to construct carbon allotropes are theoretically possible by altering the periodic binding motif in networks consisting of sp^3-, sp^2- and sp-hybridized carbon atoms [24–26]. Specifically, graphyne is a two-dimensional structure of sp–sp^2-hybridized carbon atoms (Fig. 1a), and thus graphyne can be thought of as simply replacing one-third of the carbon–carbon bonds in graphene by triple-bonded carbon linkages. The presence of these acetylenic groups in these structures introduces a rich variety of optical and electronic properties that are quite different from those of graphene or carbon nanotubes. Although significantly large molecular segments of graphyne have been experimentally synthesized [14], large regular sheets of graphyne have yet to be achieved.

2. Methodology

A series of full atomistic calculations of mechanical test cases is implemented here by classical molecular dynamics (MD) to derive a simplified set of parameters to mechanically characterize monolayer graphyne. Similar approaches have been used for the characterization of carbon nanotubes [27] and graphene systems [28]. The test suite implemented consists of the following three loading cases: (i) a stacked assembly of two sheets to determine the adhesion energy per unit area, γ, as well as effective sheet thickness, d_{vdW}; (ii) uniaxial tensile loading to determine in-plane stiffness, or Young's modulus, E, and; (iii) out-of-plane bending to determine the bending stiffness per unit width, D. The test suite is applied using a graphyne sheet of approximately 100×100 Å in dimension as depicted in Fig. 1b. The open carbon edges of graphyne are not chemically stable in ambient environment, and we terminate them covalently with hydrogen atoms. A relatively small material model of finite size (non-periodic boundary conditions) was chosen partly due to the potential synthesis of graphyne, which arise from annulene chemistry (that is, DBA precursors). As such, graphyne, unlike graphene, may be fabricated piece-wise from molecular building blocks, and achieve specimens similar in scale to our current model system and thus allowing for a direct comparison in finite-size systems.

The full atomistic investigations utilize the ReaxFF potential for carbon–carbon interactions [29,30]. The first-principles-based ReaxFF force field has been shown to provide an accurate account of the chemical and mechanical behavior of hydrocarbons, graphite, diamond, carbon nanotubes, and other carbon nanostructures [31–33] while it is capable of treating thousands of atoms with near quantum-chemical accuracy. Other reactive force fields have also been used in recent studies of the mechanics of carbon materials and may be similarly suitable for graphyne. These include the AIREBO potential [34,35] and the long-range carbon bond-order potential, LCBOPII [36], both successfully implemented in previous studies of graphene [37,38], for example. Graphyne offers a more challenging system for such potentials, as the force field must accurately capture the possibilities for bond alternation and conjugation between the acetylene and the aromatic units absent in pristine graphene systems. The version of the ReaxFF force field used here is that reported by Chenoweth et al. [29]. The time step is chosen to be on the order of a fraction of femtoseconds (0.2×10^{-15} s). It is noted that such a small time step was implemented to ensure the stability of the simulations and reflect the relatively high vibrational frequency of the triple-bonded acetylenic groups. All full atomistic simulations are subject to a microcanonical (*NVT*) ensemble, carried out at a temperature of 10 K to limit temperature fluctuations, thereby approximating molecular mechanics. Temperature control was achieved using a Berendsen thermostat [39], with a damping parameter of 100 fs (500 time steps) limiting temperature fluctuations to approximately ±1 K during dynamic simulation. All MD simulations are performed using the massively paralyzed modeling code LAMMPS (Large-scale Atomic/Molecular Massively Parallel Simulator[1]) [40] capable of running on large computing clusters. Energy minimization runs of the system are performed using a conjugate-gradient algorithm with an energy-convergence criterion implemented in the LAMMPS code. A tolerance of relative energies between minimization iterations is set at 0.0 with a force tolerance of 10^{-8} to ensure a sufficiently minimized system. As a result, energy minimization is terminated via a line-search criterion triggered by nominal atomic movement between iterations.

[1] http://lammps.sandia.gov/

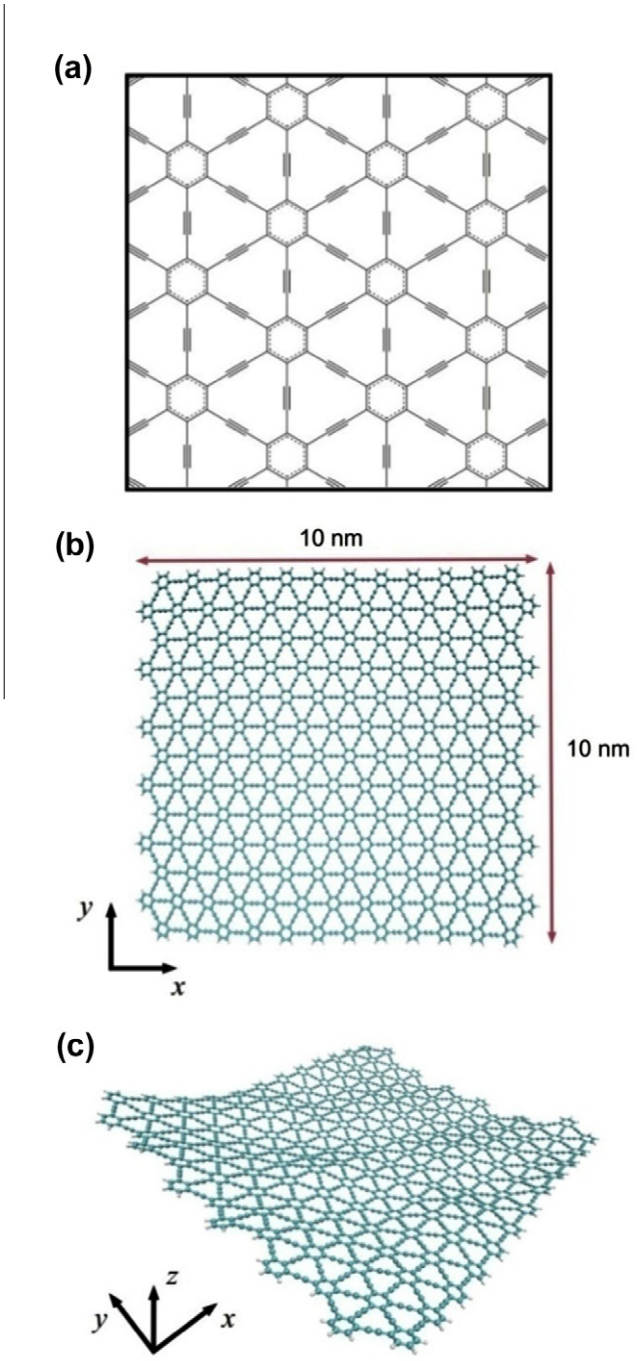

Figure 1 – Schematic of the chemical bonding structure and full atomistic model of graphyne. (a), Chemical structure graphyne, depicting uniform lattice of two-dimensional *sp*–*sp*^{2}-hybridized carbon atoms, in which aromatic carbons are bonded by single–triple–single carbon bonds. (b), Full atomistic model test specimen for mechanical characterization consisting of 10 nm by 10 nm graphyne sheet (approximately 1900 carbon atoms); boundaries terminated by hydrogen atoms. (c), Stable graphyne structure after minimization and equilibration of 0.5 ns at a temperature of 300 K.

3. Results and discussion

3.1. *Bond length analysis*

The structure acetylene linked aromatic structure of graphyne is depicted in Fig. 1. There are a number of literature reports discussing the method and basis set dependency of the degree of bond length alternation (BLA) in conjugated π-systems – DFT methods in which ReaxFF is based tend to overly favor more delocalized structures with less BLA [41–43], and thus more consistent and homogeneous bond lengths are anticipated. Being said, it has been demonstrated that optimization of various condensed aromatic compounds, including carbon annulenes, using DFT methods provides

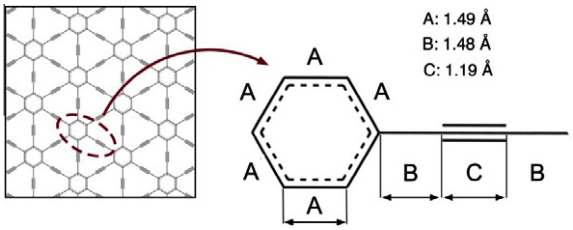

Figure 2 – Analysis of bond lengths of equilibrated and minimized graphyne structure. The bond-types in graphyne can be classified as triple and single carbon bonds (forming the acetylene linkages) between aromatic benzene rings. Bond lengths are determined by averaging values throughout the interior of the graphyne structure, resulting in near-constant values of 1.19 Å, 1.48 Å, and 1.49 Å for triple, single, and aromatic bonds, respectively (note typical values of 1.54 Å and 1.40 Å for single and aromatic bonds, respectively [45]). The presence of the acetylene groups have been shown to reduce the aromatic character of the benzene ring, where the length of the shared bond between the acetylene groups and the benzene ring is elongated due to weak conjugation between the two alkyne units.

results in excellent agreement with experimental data [44]. We analyze the obtained equilibrated and minimized structure based on the three constituent bonds which we label triple, single, and aromatic (see Fig. 2).

Direct bond length measurements are taken from the energy minimized graphyne sheet. A random selection of bond lengths from the interior section is average, resulting in near-constant values of 1.19 Å, 1.48 Å, and 1.49 Å for triple, single, and aromatic bonds respectively.

Bond alternation is one of the traditional criteria for the aromaticity of conjugated ring systems [46,47]. The carbon–carbon bond distances of the triple bonds of DBA structures has been shown to be virtually constant (1.215–1.216 Å), and the same is true for the single bond lengths (1.418–1.423 Å), with notable difference of the bond lengths observed in the benzene rings [13]. The benzene rings of smaller DBA structures vary in bond length from 1.417 to 1.427 Å for interior rings [13]. The current study depicts longer bond lengths of both the single and aromatic bonds. Qualitatively, the presence of the acetylene groups have been shown to reduce the aromatic character of the benzene ring, where the length of the shared bond between the acetylene groups and the benzene ring is elongated presumably due to weak conjugation between the two alkyne units and the benzene ring. The current structure seems to be reflective of this effect wherein the single bonds have contracted and the aromatic bonds extended compared to typical values (from approximately 1.54 Å and 1.40 Å, respectively [45]).

3.2. *Adhesion energy and interlayer spacing*

We first characterize weak interactions (i.e. primarily van der Waals interactions) between two graphyne surfaces. For adhesion simulations, two copied graphyne sheets are simulated together and moved into close proximity to one another while calculating the potential energy over the range of

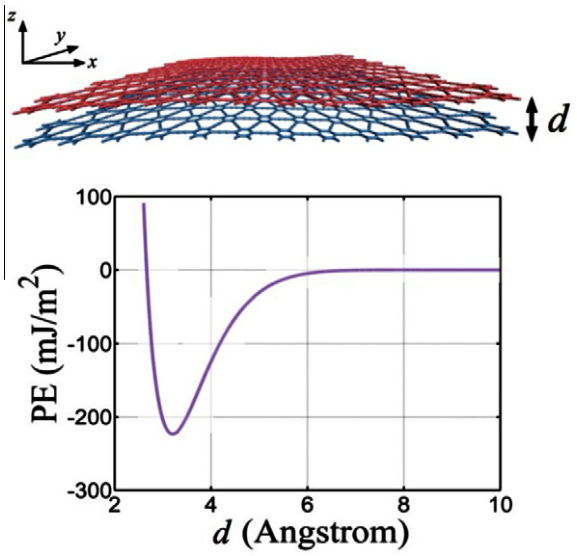

Figure 3 – Determination of interlayer adhesion in graphyne. Two identical sheets of graphyne, free to move in the *xy*-plane, are brought into proximity by a constant velocity along the *z*-axis (upper panel). The total potential energy and average sheet separation, *d*, is tracked during the process. We plot the potential energy versus intersheet distance, *d*, and find an equilibrium spacing of d_{vdW} = 3.20 Å and surface energy of γ = 223.5 mJ/m^2 (lower panel).

distances (Fig. 3). The geometric configuration at contact (energy minima) can be used to determine equilibrium distances,

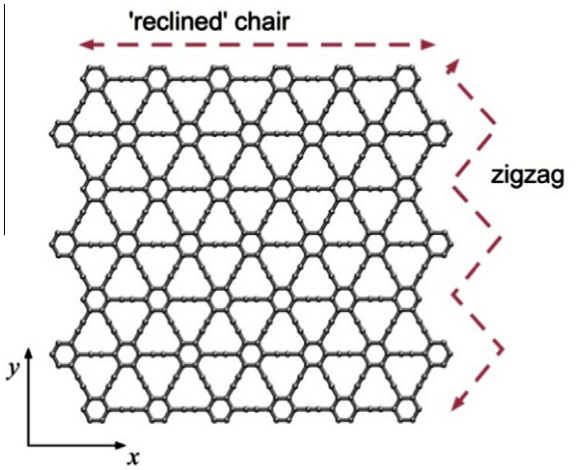

Figure 4 – Definition of the geometry of graphyne edges. The edges of graphene are designated *armchair* or *zigzag* based on the orientation of the hexagonal crystalline lattice. Similarly, graphyne is constructed from a hexagonal supercell, and exhibits characteristic zigzag edges (oriented along the y-axis). However, due to the triple-bond linkages, the expected armchair edges are characterized by a more linear topology of repeating acetylenic and aromatic units (as opposed to offset aromatic units of graphene). We thus define these edges as *'reclined'-chair* to share the vernacular of graphene and reflect the flattened topology.

while the differences in energy minima between the equilibrium distance and at a semi-infinite separation can be used to extract potential energy gain of adhesion per unit area (Fig. 3).

We find an equilibrium distance, d_{vdW}, of 3.20 Å, with a surface energy, γ, approximately 223.5 mJ/m^2. It was previously predicted by a first-principles atomic orbital method that the equilibrium interlayer distance would exceed that of graphite/graphene [48] – however, the determined interlayer distance of 3.20 Å is slightly less than the common accepted value of 3.35 Å for graphene/graphite. This difference can potentially be attributed to the more sparse arrangement of carbon atoms within the graphyne sheet, resulting in a weaker surface energy landscape and thus closer equilibrium contact between layers. Moreover, previous computational and experimental investigations of graphene indicate adhesion energies from 260 to 345 mJ/m^2 [28,49,50]. The smaller value of 223.5 mJ/m^2 found here for graphyne is consistent with the sparser layout of in-plane carbon atoms per sheet. For comparison, it has been reported that the spatulae of a gecko – noted for its dry-adhesion capabilities – has adhesion energies on the order of 48.6–62.5 mJ/m^2 [51].

3.3. *Uniaxial tension: stiffness, ultimate stress and ultimate strain*

It is well established that the strain energy and deformation of graphene sheets can be described by continuum elasticity theory [52–57], as such the same assumptions are applied to graphyne. For the current mechanical characterization, it is assumed that under small deformation graphyne can be approximated as a linear elastic material. Further, to take advantage of the two-dimensional planar arrangement, a plane stress approximation is utilized to calculate mechanical parameters [58]. More complex elasticity models can be implemented to account for out-of-plane behavior, aniso-

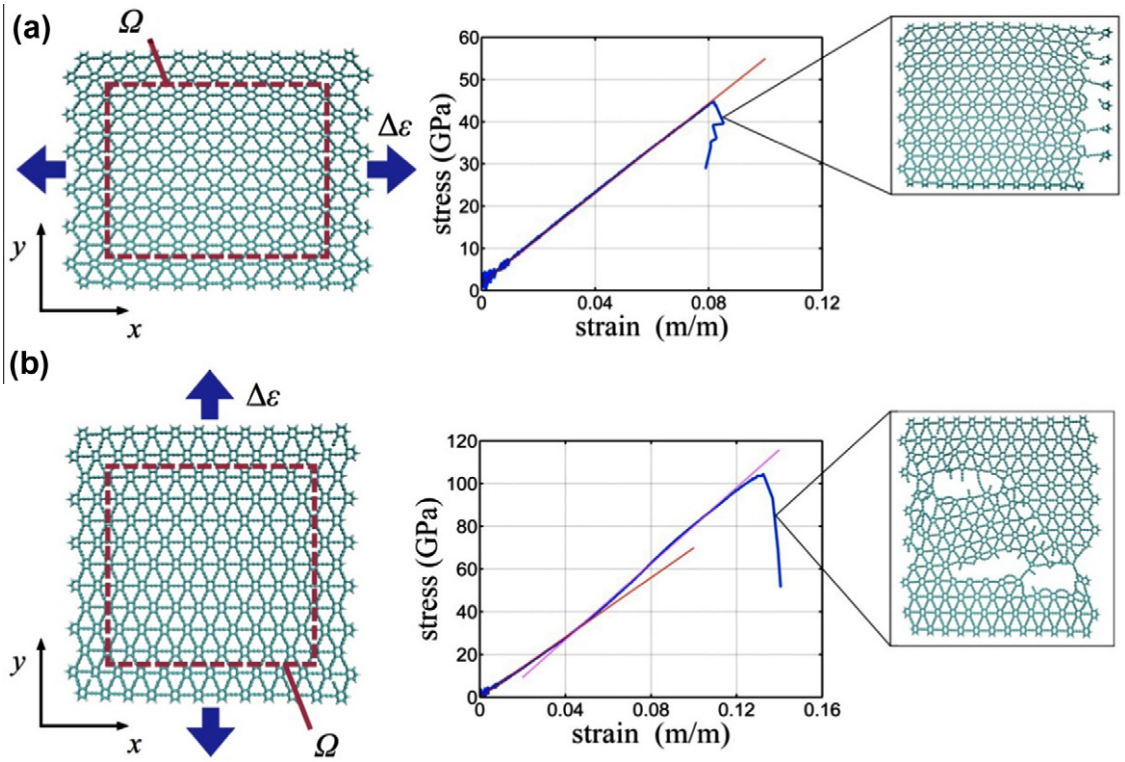

Figure 5 – Schematic and stress–strain results of uniaxial tension tests, in reclined-chair (*x*-axis) and zigzag (*y*-axis) directions. (a), Reclined-chair direction; uniform strain was applied by displacing the graphyne edges in the *x*-direction at a constant velocity. The virial stress is calculated over a representative volume, Ω, chosen within the interior of the graphyne sheet to avoid boundary effects. For volume calculations we assume a thickness of 3.20 Å, taken from adhesion energy results (Fig. 3). Fitting the resulting stress–strain data, a Young's modulus of 532.5 GPa is calculated (or 170.4 N/m without consideration of the sheet thickness), with an ultimate stress of 48.2 GPa and maximum strain of 0.0819. Failure is found to be localized to a single edge. (b), Zigzag direction; uniform strain is applied by displacing the graphyne edges in the *y*-direction at a constant velocity. As before, the virial stress is calculated over the same representative volume, Ω, assuming a thickness of 3.20 Å (Fig. 3). Fitting the resulting stress–strain data, an initial stiffness of 700.0 GPa is calculated (or 224.0 N/m without consideration for sheet thickness). The strain along the zigzag direction results in a stiffening behavior, with an increase of the tangent modulus to 888.4 GPa (284.3 N/m), or 27% increase over the small-deformation modulus. The mechanistic reason for this increase is that the acetylenic groups align towards the applied strain, resulting in higher sustained stress and strain. An ultimate stress of 107.5 GPa and strain of 0.1324 is determined at failure, which is characterized by multiple fracture sites.

tropic and finite strain effects, but are beyond the scope of the current investigation. Graphyne, like graphene, has an in-plane hexagonal symmetry [10]. The edges of graphene are traditionally designated *armchair* or *zigzag* based on the orientation of the hexagonal crystalline lattice. Similarly, as graphyne is constructed from a hexagonal supercell it exhibits characteristic zigzag edges. However, due to the triple-bond linkages, the expected armchair edges are characterized by a linear topology of repeating acetylenic and aromatic units (as opposed to offset aromatic units of graphene). We thus define these edges as '*reclined*'-*chair* to share the common vernacular of graphene while reflecting the flattened topology (Fig. 4).

Two uniaxial tensile tests are applied to the graphyne sheet by fixing the boundaries in the desired direction and deforming the unit cell by stretching along either the *x*- or y-directions at a uniform rate (thereby inducing a uniform strain rate). It is noted that the fixed edges are free to move orthogonal to the applied strain. Non-periodic boundary conditions result in a graphyne sheet of finite size. To limit the effects of the boundaries, all stress and energies considered are derived from an interior representative volume of the sheet. Due to the relatively small time step, the strain rate applied is $5.0 \times 10^8\ s^{-1}$ (a velocity of approximately 5 m/s). It is noted that strain rates of 10 m/s, 1 m/s, and 0.5 m/s are utilized to explore any rate dependence with minimal differences in results. The virial stress is commonly used to relate to the macroscopic (continuum) stress in molecular dynamics computations [59,60]. The virial stress approach allows us to determine the components of the macroscopic stress tensor, S_{ij} in a volume Ω. To reduce random and temperature-related stress fluctuations, in addition to averaging over the representative volume, Ω, the stress is averaged further over a small time interval of 100 fs around the desired time point of stress calculation. To calculate the total stress, $\sigma_{ij} = S_{ij}\Omega^{-1}$ where Ω is taken as the dimensions of the interior portion of the graphyne sheet free from imposed boundary conditions.

The ambiguity for the thickness of mono-atomic crystal structures such as graphyne, graphene and carbon nanotubes has been discussed in a previous study [61], suggesting the stress and elastic moduli of monolayer graphene be reported in force per unit length (N/m) rather than force per unit area (N/m^2 or Pa). Here, the label of "Young's modulus" is only intended as a placeholder for the in-plane tensile stiffness of graphyne. In agreement with previous investigations, we assert that the continuum interpretation of Young's modulus, *E*, is not reflective of monolayer graphyne, and is merely used here as a convenient convention for comparison. Through the use of common terms, more apt assessment can be made with previous (and future) studies and with other material systems.

The graphyne sheet is strained to 25%, which was chosen to encompass the deformation until fracture. The resulting stress–strain relationships can then be plotted (Fig. 5). From the plane stress assumption, it can be shown that, $\varepsilon_x = (1/E)[\sigma_x - \nu_p\sigma_y]$ where *E* is the desired Young's modulus. From the results of the full atomistic simulations, for uniaxial strain, $\sigma_x \gg \sigma_x$ thus we arrive at two simple linear elastic relations: $\sigma_x = E{\cdot}\varepsilon_x$ (and similarly in the y-direction). For non-periodic boundaries, the free edges effectively limit $\sigma_y \approx 0$ and

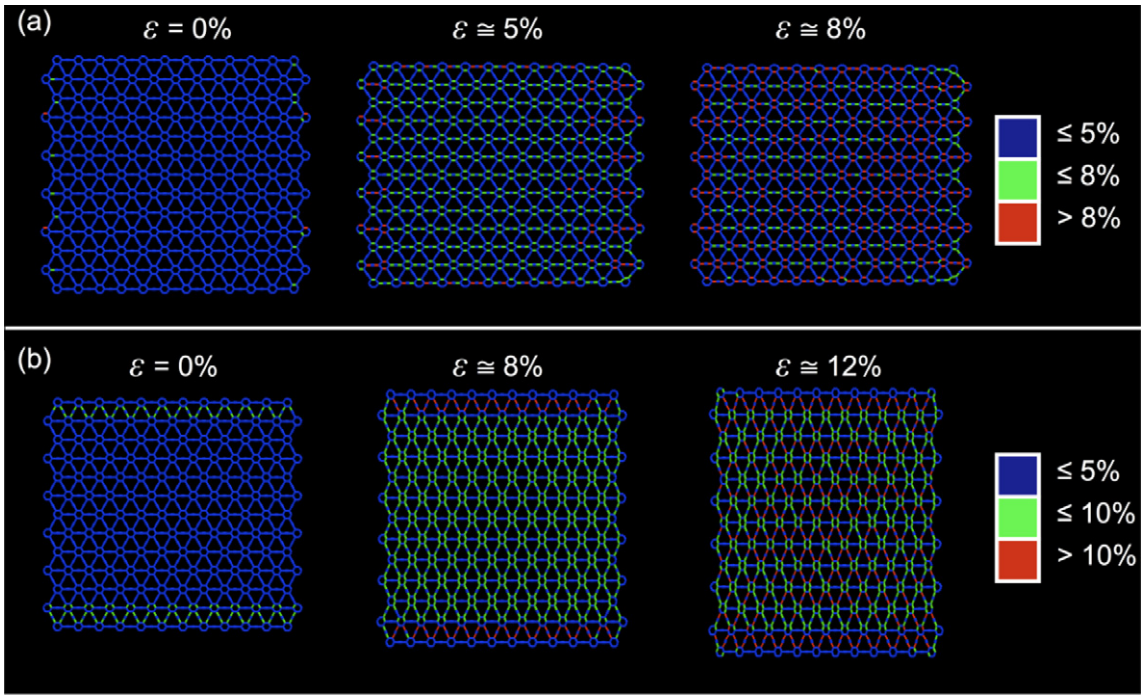

Figure 6 – Bond strain distributions for uniaxial tension tests in (a) reclined-chair and (b) zigzag directions. In both cases, the bulk of the deformation (and thus highest strain) is undertaken by the single carbon bonds aligned with the direction of strain, followed by the sections of the aromatic rings aligned with the strain, and nominal strain experienced by the relatively stiff triple bonds. The strain field is relatively homogenous throughout the interior of the graphyne sheet. Note that at zero applied strain, the present nonzero local strain is attributed to the fixed boundary conditions.

biaxial effects are neglected. Thus, the derived stiffness should be considered uniaxial stiffness only. The simulation results in a Young's modulus value of approximately 532.5 GPa for uniaxial strain along the reclined-chair direction (*x*-axis). Assuming a thickness equivalent to the van der Waals spacing, 3.20 Å (a common assumption associated with graphene) results in a moduli of 170.4 N/m for tension along the *x*-axis. The ultimate strain under tension was taken as the strain level at maximum stress (ε_{ult} = 0.0819 at 48.2 GPa; see Fig. 5a). It is noted that the ultimate strain does not necessarily represent the complete fracture of the graphyne sheet, but merely local rupture and subsequent drop in load capacity.

The triple-bonded acetylenic groups are directly subject to strain applied in the reclined-chair direction, leading to reductions in both stress and strain capacity. Uniaxial strain along the zigzag direction (y-axis) results in stiffening behavior (Fig. 5b). Considering only the initial regime (up to approximately 5% strain), we determine a stiffness of 700.0 GPa (or 224.0 N/m). Upon additional applied strain, the triple-bonded acetylenic groups undergo alignment to the direction of strain, and stiffness is increased to 888.4 GPa (284.3 N/m) – an increase of approximately 27%. Subsequently, more engaged carbon bonds facilitate an increase in stress, and the internal realignment increases strain capacity, resulting in ultimate values of 107.5 GPa and 0.1324, respectively.

Covalently bonded graphyne mechanistically behaves as an atomistic spring-system (albeit nonlinearly). It is expected that maximum strain and therefore failure (bond rupture) will occur at the single-bonded sections of the acetylene units. An inspection of the failed bonds reveals rupture did occur at the carbon–carbon single bonds when strained along both the zigzag and reclined-chair directions (Fig. 6). A bond length analysis of uniaxial stretching in the reclined-chair direction (Fig. 6a) reveals nominal strain experienced by the triple bonds (lengths in the range of 1.18–1.20 Å at 8.1% strain just prior to rupture). Aromatic bonds aligned with the direction of strain had lengths of 1.54–1.55 Å, or a strain of approximately 3–4% prior to rupture. The single bonds aligned with the strain, however, had lengths on the order of 1.55–1.64 Å (approximately 5–11% strain), attributing the bulk of deformation. Nonaligned bonds of all types depicted nominal strain.

An inspection of the bond lengths during uniaxial stretching in the zigzag direction (Fig. 6b) again reveals nominal strain experienced by the triple bonds (lengths in the range of 1.18–1.21 Å at 13.2% strain just prior to rupture). Again, aromatic bonds aligned with the direction of strain had lengths of 1.54–1.55 Å, or a strain of approximately 3–4% prior to rupture, whereas single bonds aligned with the strain had lengths on the order of 1.59–1.72 Å (approximately 7–17% strain). Nonaligned bonds (those parallel to the reclined-chair direction), however, did not depict nominal strain – they were subject to shortening (compressive strain) by 3–4%. Such compression-like behavior was likely facilitated by the low temperature conditions, which limited atomistic motions that would likely lead to local buckling (rippling) of the sheet. Such behavior also supports the observed anisotropic behavior, wherein the stiffening effect is attributed to the energy required to compress the graphyne sheet in-plane orthogonal to the applied strain.

To corroborate the results of virial stress through an applied constant strain rate, and eliminate any potential rate dependence, we also determine the in-plane stiffness by an energy minimization approach. Affine strain is applied to the graphyne system and subsequently minimized while computing the elastic energy density (potential energy per unit volume). The application of incremental strain followed by energy minimization is a quasi-static methodology that circumvents strain rate effects. Such an approach requires system minimization at discrete strain values, and is thus more computationally expensive than an applied uniform strain rate. While rate dependence is avoided, it is more difficult to observe dynamic failure phenomena at ultimate stresses, but can provide more physical derivations of stiffness.

The associated Young's modulus was calculated by fitting the energy-strain data to the following expression: $U_{tens} = 1/2E\varepsilon^2$, where U_{tens} is the system strain energy per unit volume, E is the modulus, and ε is the prescribed uniaxial strain (Fig. 7). Again, the volume is calculated by assuming a thickness equivalent to the van der Waals spacing, or 3.20 Å. This approach results in a Young's modulus value of 629.4 GPa along the reclined-chair direction (with an R^2 value exceeding 0.99), and failure at approximately 8% strain and an ultimate stress of 44.8 GPa. For the zigzag direction, again there was an onset of stiffening, resulting in a small strain stiffness of 772.0 GPa and a large strain stiffness of 964.4 GPa (for

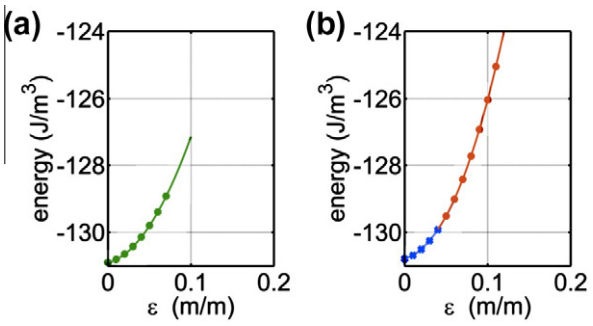

Figure 7 – Determination of in-plane tensile stiffness by energy minimization for (a) reclined-chair and (b) zigzag directions. Young's modulus is calculated by fitting the energy-curvature data to the following expression: $U_{tens} = 1/2E\varepsilon^2$, where U_{tens} is the system potential energy per unit volume, E is the modulus. Applied strains of 0.01–0.20 are imposed on the graphyne system and the minimized energies plotted versus ε. This approach results in a Young's modulus value of 629.4 GPa along the reclined-chair direction (with an R^2 value exceeding 0.99), with failure at a strain of 0.08 at a stress of 44.8 GPa (failure at 0.0819 strain at 48.2 GPa under constant strain rate; see Fig. 5). For the zigzag direction, as before in the finite temperature calculations we identify an onset of stiffening, resulting in a small strain stiffness of 772.0 GPa and a large strain stiffness of 964.4 GPa (for $\varepsilon > 0.05$), with failure at a strain of 0.12 at a stress of 99.9 GPa (compared to a ultimate strain of 0.1324 and 107.5 GPa under constant strain rate; Fig. 5). The results of the energy minimization approach depict slightly higher stiffness as compared with the constant strain-rate results, as well as nominal decreases in the ultimate stress and strain values.

$\varepsilon > 0.05$). Failure occurred at approximately 12% strain at an ultimate stress of 99.9 GPa. The results of the energy minimization approach depict a slightly higher stiffness as compared with the constant strain-rate results, as well as nominal decreases in the ultimate stress and strain (due to the discrete application of strain for the energy method, more exact values of ultimate strain are difficult to determine). Future studies with variation in applied strain rates and temperature may deviate from the results predicted here, but presumably within a marginal range, and distinct anisotropic behavior of graphyne is clearly indicated.

Previous investigations determined Young's modulus of a single layer graphene sheet is reported on the order of approximately 1 TPa (335 N/m) with negligible difference between armchair and zigzag orientations [62–66]. From the current results, graphyne is about one half the stiffness of graphene along the reclined-chair direction, but approaches the stiffness in the zigzag direction. Previous computational and experimental studies [65–68] report ultimate stress and strain for graphene under tension are approximately 130 GPa at 20% strain. Thus, the mechanical performance of graphyne is slightly inferior to graphene in terms of stiffness, strength, and ductility. It is noted, however, the sheet areal density of graphyne (approximately 0.54 mg/m^2) is less than that of graphene (approximately 0.8 mg/m^2), calculated simply by explicitly accounting for the atomic mass of the constituent carbons over a representative area. Subsequently, the surface area of monolayer graphyne is on the order of 3600 m^2/g, which exceeds even that of graphene (2500 m^2/g), deemed beneficial to potential energy storage applications [69] as well as accessible area for possible chemical functionalization [70].

3.4. *Bending stiffness*

Theoretical studies and synthesis [37,71] have suggested that bending stiffness of monolayer graphene is critical in attaining the structural stability and morphology of graphene sheets, which in turn could have important impacts on their electronic properties. This would similarly hold for other 2D crystal structures such as graphyne. Moreover, like graphene, graphyne is also a membrane material in nature, which has a very low resistance to bending. Due to the relative flexibility and single atom thickness of monolayer graphyne, a mechanical bending test is difficult to implement [61,65] – it is very difficult to apply a bending moment directly to such structures as local bending on a membrane structure would induce local curvature only. To circumvent this issue, the isotropic bending modulus is determined by one-dimensional pure bending experiments using molecular statics in which curvature is induced (and fixed) prior to energy minimization, similar to previous coarse-grain [28] and full atomistic [55,72,73] investigations.

To calculate the bending modulus of graphyne, the same rectangular sheet is now bent into a section of a cylinder with constant radius of curvature throughout the basal plane (Fig. 8a and b). The neutral plane for pure bending is parallel to the layer and passes through the centroid of the bending cross section. The edges of the bent sheet are kept fixed and the bulk of the sheet is allowed to relax to an energy minimum. To avoid boundary effects at the fixed edges, the elastic energy is only considered for the interior portion of the graphyne sheet (Fig. 8b). At finite temperatures, like graphene, graphyne exhibits ripples and undulations out-of-plane (see Fig. 1c for example). As such, the graphyne structure deviates from the ideal curvature initial imposed and we the derived stiffness can be considered the effective bending modulus. However, both the low temperature equilibrium and minimization process limit the observed ripples, and the system curvature is maintained (Fig. 8b depicts and equilibrated and minimized structure).

The bending modulus is calculated by fitting the energy-curvature data to the following expression [74]: $U_{bend} = 1/2\ D\ \kappa^2$, where U_{bend} is the system strain energy per unit basal plane area, D is the bending modulus per unit width, and κ is the prescribed beam curvature. Curvatures in the range of

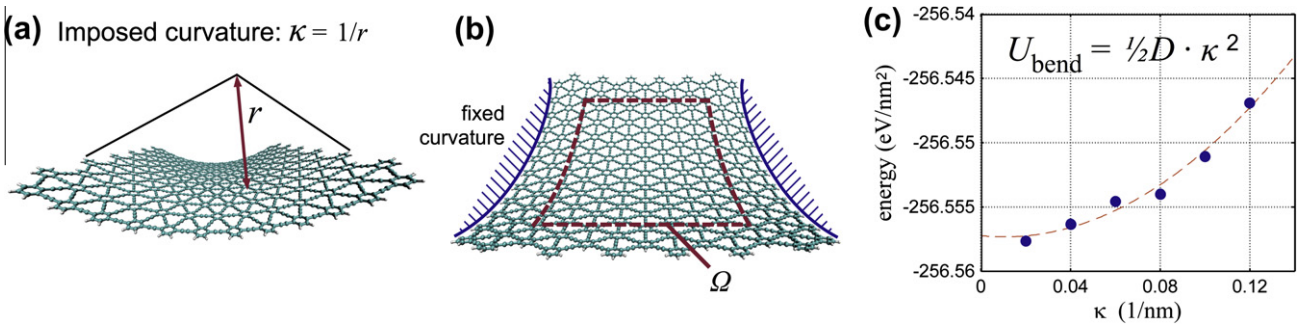

Figure 8 – Determination of out-of-plane bending stiffness. (a), A graphyne sheet bent into a section of a cylinder with an imposed constant radius of curvature, $\kappa = \frac{1}{r}$, throughout the basal plane. (b) Depiction of boundary conditions wherein the edges of the bent sheet are kept fixed and the bulk of the sheet is allowed to relax to an energy minimum; only interior representative volume, Ω, considered for energy calculation to limit boundary effects; depicted structure is after equilibration and minimization for $\kappa = 0.012$ Å^{-1}. (c), The bending modulus is calculated by fitting the energy-curvature data to the following expression: $U_{bend} = 1/2D\ \kappa^2$, where U_{bend} is the system strain energy per unit basal plane area, D is the bending modulus per unit width. Curvatures of 0.002–0.012 Å^{-1} (cylindrical radii of approx. 83–500 Å) are imposed on the graphyne system and the minimized energies plotted versus κ. The resulting bending stiffness is calculated to be approximately 1.68 eV (with an R^2 value of 0.98).

Table 1 – Summary of mechanical properties of graphyne.

Property	Value	Unit
Interlayer equilibrium spacing, d_{vdW}	3.20	Å
Surface energy, γ	223.5	mJ/m^2
Bending stiffness per unit width, D	2.69(10^{-19})	J
Reclined-chair direction		
Modulus (stiffness)		
Constant strain rate	532.5 (170.4)	GPa (N/m)
Energy minimization	629.4 (201.4)	GPa (N/m)
Ultimate stress		
Constant strain rate	48.2	GPa
Energy minimization	44.8	GPa
Ultimate strain		
Constant strain rate	8.19	%
Energy minimization	8	%
Zigzag Direction		
Small strain modulus (stiffness)		
Constant strain rate	700.0 (224.0)	GPa (N/m)
Energy minimization	772.0 (247.0)	GPa (N/m)
Large strain modulus (stiffness)		
Constant strain rate	888.4 (284.3)	GPa (N/m)
Energy minimization	964.4 (308.6)	GPa (N/m)
Ultimate stress		
Constant strain rate	107.5	GPa
Energy minimization	99.9	GPa
Ultimate strain		
Constant strain rate	13.24	%
Energy minimization	12	%

0.002–0.012 Å^{-1} (cylindrical radii of approx. 83–500 Å) are imposed on the graphyne system and the minimized energies are plotted versus κ (Fig. 8c).

The resulting bending stiffness is calculated to be approximately 2.69×10^{-19} J (or 1.68 eV), with an R^2 value of 0.98. In comparison to monolayer graphene, previous investigations report values of bending stiffness ranging from 0.69 to 2.1 eV [55,64,65,72,73], dependent on technique (*ab initio*, MD, etc.) and the chosen potential, with values on the order of 1.4–1.5 eV being typically accepted [64,73]. This result indicates that graphyene, due to the relative bending stiffness of the triple-bonded linkages, achieves a remarkable bending stiffness on the order of graphene, with less atomic density. The relative flexibility of graphyne, like graphene, indicates the possibility of graphyne-based nanotubes. Indeed, the theoretical structure and stability of such nanotubes has previously been investigated through tight-binding and *ab initio* density functional methods [21]. Table 1 summarizes the results of all atomistic simulations reported here in an overview.

4. Conclusion

The intensive study of carbon nanotubes and graphene has now paved the way for the next step in the evolution of carbon materials. Progress in carbon nanotube and graphene science has been driven by the theoretical predictions from first-principles-based simulations which were tested with experimental work, and vice versa. Similarly, the motivation for the determination of the properties of novel materials such as graphyne leads to important insights that drive the development of new models and experimental assays to probe this material. The work reported here could help us to determine whether or not the pursuit of synthesis and characterization of graphyne-type carbon is worthwhile. Currently, to the best of our knowledge, there are no empirical results on the mechanical properties of graphyne-like molecular structures, thereby limiting direct comparisons to known carbon allotropes, such as graphene.

Our results show that this material has indeed interesting mechanical properties that differ in important aspects from those of graphene, which can be important from an engineering design point of view. Our work also provides generic insight that can be applied to similar molecular substructures for the potential design of *de novo* material systems, such as other types of two-dimensional crystals that may exist [75]. Indeed, many properties of graphene were known from theoretical point of view before it was possible to perform actual measurements. The superlative properties of mono- and multilayer graphyne sheets identified here may facilitate the design of advanced composites with superior mechanical and electrical performance where in particular the concept of functionalization, enabled by the particular structure of graphyne, may provide exciting opportunities.

Acknowledgements

This work was supported primarily by the MRSEC Program of the National Science Foundation under award number DMR-0819762. The calculations and the analysis were carried out using a parallelelized LINUX cluster at MIT's Laboratory for Atomistic and Molecular Mechanics (LAMM). Visualization

has been carried out using the VMD visualization package [76]. We recognize Professor Eduardo Kausel (MIT) for providing the impetus of investigation.

REFERENCES

[1] Kroto HW, Heath JR, O'Brien SC, Curl RF, Smalley RE. C-60 - Buckminsterfullerene. Nature 1985;318(6042):162–3.
[2] Iijima S. Helical Microtubules of Graphitic Carbon. Nature 1991;354(6348):56–8.
[3] Novoselov KS, Geim AK, Morozov SV, Jiang D, Zhang Y, Dubonos SV, et al. Electric field effect in atomically thin carbon films. Science 2004;306(5296):666–9.
[4] Chalifoux WA, Tykwinski RR. Synthesis of polyynes to model the sp-carbon allotrope carbyne. Nat Chem 2010;2(11):967–71.
[5] Li GX, Li YL, Liu HB, Guo YB, Li YJ, Zhu DB. Architecture of graphdiyne nanoscale films. Chem Commun 2010;46(19):3256–8.
[6] Sheng X-L, Yan Q-B, Ye F, Zheng Q-R, Su G. T-carbon: a novel carbon allotrope. Phys Rev Lett 2011;106:155703.
[7] Minyaev RM, Avakyan VE. Supertetrahedrane-A new possible carbon allotrope. Dokl Chem 2010;434:253–6.
[8] Falcao EHL, Wudl F. Carbon allotropes: beyond graphite and diamond. J Chem Technol Biotechnol 2007;82(6):524–31.
[9] Hirsch A. The era of carbon allotropes. Nat Mater 2010;9(11):868–71.
[10] Baughman RH, Eckhardt H, Kertesz M. Structure-property predictions for new planar forms of carbon – layered phases containing Sp2 and Sp atoms. J Chem Phys 1987;87(11):6687–99.
[11] Narita N, Nagai S, Suzuki S, Nakao K. Optimized geometries and electronic structures of graphyne and its family. Phys Rev B 1998;58(16):11009–14.
[12] Grima JN, Evans KE. Self expanding molecular networks. Chem Commun 2000(16):1531–2.
[13] Tahara K, Yoshimura T, Sonoda M, Tobe Y, Williams RV. Theoretical studies on graphyne substructures: Geometry, aromaticity, and electronic properties of the multiply fused dehydrobenzo[12]annulenes. J Org Chem 2007;72(4):1437–42.
[14] Haley MM. Synthesis and properties of annulenic subunits of graphyne and graphdiyne nanoarchitectures. Pure Appl Chem 2008;80(3):519–32.
[15] Pan LD, Zhang LZ, Song BQ, Du SX, Gao H-J. Graphyne- and graphdiyne-based nanoribbons: density functional theory calculations of electronic structures. Appl Phys Lett 2011;98:173102.
[16] Marsden JA, Palmer GJ, Haley MM. Synthetic strategies for dehydrobenzo[n]annulenes. Eur J Org Chem 2003;23(13):2355–69.
[17] Tahara K, Yoshimura T, Ohno M, Sonoda M, Tobe Y. Syntheses and photophysical properties of boomerang-shaped bis(dehydrobenzo[12]annulene) and trapezoid-shaped tris(dehydrobenzo[12]annulene). Chem Lett 2007;36(7):838–9.
[18] Kehoe JM, Kiley JH, English JJ, Johnson CA, Petersen RC, Haley MM. Carbon networks based on dehydrobenzoannulenes. 3. Synthesis of graphyne substructures. Org Lett 2000;2(7):969–72.
[19] Spitler EL, Johnson CA, Haley MM. Renaissance of annulene chemistry. Chem Rev 2006;106(12):5344–86.
[20] Stevenson CD. Annulenylenes, annulynes, and annulenes. Acc Chem Res 2007;40(8):703–11.
[21] Coluci VR, Braga SF, Legoas SB, Galvao DS, Baughman RH. New families of carbon nanotubes based on graphyne motifs. Nanotechnology 2004;15(4):S142–9.
[22] Bhaskar A, Guda R, Haley MM, Goodson T. Building symmetric two-dimensional two-photon materials. J Am Chem Soc 2006;128(43):13972–3.
[23] Tahara K, Fujita T, Sonoda M, Shiro M, Tobe Y. Donors and Acceptors Based on Triangular Dehydrobenzo[12]annulenes: Formation of a Triple-Layered Rosette Structure by a Charge-Transfer Complex. J Am Chem Soc 2008;130(43):14339–45.
[24] Diederich F, Kivala M. All-Carbon Scaffolds by Rational Design. Adv Mater 2010;22(7):803–12.
[25] Karfunkel HR, Dressler T. New hypothetical carbon allotropes of remarkable stability estimated by modified neglect of diatomic overlap solid-state self-consistent field computations. J Am Chem Soc 1992;114(7):2285–8.
[26] Diederich F, Rubin Y. Synthetic approaches toward molecular and polymeric carbon allotropes. Angew Chem, Int Ed Engl 1992;31(9):1101–23.
[27] Buehler MJ. Mesoscale modeling of mechanics of carbon nanotubes: self-assembly, self-folding and fracture. J Mater Res 2006;21(11):2855–69.
[28] Cranford S, Sen D, Buehler MJ. Meso-origami: folding multilayer graphene sheets. Appl Phys Lett 2009;95(12):123121.
[29] Chenoweth K, van Duin ACT, Goddard WA. ReaxFF reactive force field for molecular dynamics simulations of hydrocarbon oxidation. J Phys Chem A 2008;112(5):1040–53.
[30] Strachan A, Kober EM, van Duin ACT, Oxgaard J, Goddard WA. Thermal decomposition of RDX from reactive molecular dynamics. J Chem Phys 2005;122(5):054502.
[31] van Duin ACT, Dasgupta S, Lorant F, Goddard WA. ReaxFF: a reactive force field for hydrocarbons. J Phys Chem A 2001;105(41):9396–409.
[32] Nielson KD, van Duin ACT, Oxgaard J, Deng WQ, Goddard WA. Development of the ReaxFF reactive force field for describing transition metal catalyzed reactions, with application to the initial stages of the catalytic formation of carbon nanotubes. J Phys Chem A 2005;109(3):493–9.
[33] Chen N, Lusk MT, van Duin ACT, Goddard WA. Mechanical properties of connected carbon nanorings via molecular dynamics simulation. Phys Rev B 2005;72(8):085416.
[34] Stuart SJ, Tutein AB, Harrison JA. A reactive potential for hydrocarbons with intermolecular interactions. J Chem Phys 2000;112(14):6472–86.
[35] Brenner DW, Shenderova OA, Harrison JA, Stuart SJ, Ni B, Sinnott SB. A second-generation reactive empirical bond order (REBO) potential energy expression for hydrocarbons. J Phys: Condens Matter 2002;14(4):783–802.
[36] Los JH, Ghiringhelli LM, Meijer EJ, Fasolino A. Improved long-range reactive bond-order potential for carbon *I. Construction*. Phys Rev B 2005;72:214102 (21).
[37] Fasolino A, Los JH, Katsnelson MI. Intrinsic ripples in graphene. Nat Mater 2007;6(11):858–61.
[38] Shenoy VB, Reddy CD, Ramasubramaniam A, Zhang YW. Edge-stress-induced warping of graphene sheets and nanoribbons. Phys Rev Lett 2008;101(24):245501.
[39] Berendsen HJC, Postma JPM, Vangunsteren WF, Dinola A, Haak JR. Molecular-dynamics with coupling to an external bath. J Chem Phys 1984;81(8):3684–90.
[40] Plimpton SJ. Fast parallel algorithms for short-range molecular dynamics. J Comput Phys 1995;117:1–19.
[41] King RA, Crawford TD, Stanton JF, Schaefer HF. Conformations of [10]annulene: More bad news for density functional theory and second-order perturbation theory. J Am Chem Soc 1999;121(46):10788–93.
[42] Choi CH, Kertesz M. New interpretation of the valence tautomerism of 1, 6-methano[10]annulenes and its application to fullerene derivatives. J Phys Chem A 1998;102(19):3429–37.

[43] Petrukhina MA, Andreini KW, Mack J, Scott LT. X-ray quality geometries of geodesic polyarenes from theoretical calculations: what levels of theory are reliable? J Org Chem 2005;70(14):5713–6.
[44] Williams RV, Armantrout JR, Twamley B, Mitchell RH, Ward TR, Bandyopadhyay S. A theoretical and experimental scale of aromaticity. The first nucleus-independent chemical shifts (NICS) study of the dimethyldihydropyrene nucleus. J Am Chem Soc 2002;124(45):13495–505.
[45] Haynes WM. Handbook of chemistry and physics. 91st ed. CRC Press; 2010.
[46] Minkin VI, Glukhovtsev MN, Simkin BIA, *Aromaticity and antiaromaticity:* electronic and structural aspects. 1994; New York: Wiley. xiii, p.313
[47] Krygowski TM, Cyranski MK. Structural aspects of aromaticity. Chem Rev 2001;101(5):1385–419.
[48] Narita N, Nagai S, Suzuki S, Nakao K. Electronic structure of three-dimensional graphyne. Phys Rev B 2000;62(16):11146–51.
[49] Henry DJ, Yiapanis G, Evans E, Yarovsky I. Adhesion between graphite and modified polyester surfaces: a theoretical study. J Phys Chem B 2005;109:17224–31.
[50] Girifalco LA, Lad RA. Energy of cohesion, compressibility, and the potential energy functions of the graphite system. J Chem Phys 1956;25(4):693–7.
[51] Autumn K, Sitti M, Liang YCA, Peattie AM, Hansen WR, Sponberg S, et al. Evidence for van der Waals adhesion in gecko setae. Proc Natl Acad Sci USA 2002;99(19): 12252–6.
[52] Robertson DH, Brenner DW, Mintmire JW. Energetics of nanoscale graphite tubules. Phys Rev B 1992;45(21): 12592–5.
[53] Tomanck D, Zhong W, Krastev E. Stability of multishell fullerenes. Phys Rev B 1993;48(20):15461–4.
[54] Ruoff RS, Qian D, Liu WK. Mechanical properties of carbon nanotubes: theoretical predictions and experimental measurements. C.R. Phys 2003;4:993–1008.
[55] Lu Q, Huang R. Nonlinear Mechanicas of Single-Atomic-Layer Graphene Sheets. Int J Appl Mech 2009;1(3):443–67.
[56] Zhou J, Huang R. Internal lattice relaxation of single-layer graphene under in-plane deformation. J Mech Phys Solids 2008;56(4):1609–23.
[57] Wei XD, Fragneaud B, Marianetti CA, Kysar JW. Nonlinear elastic behavior of graphene: Ab initio calculations to continuum description. Phys Rev B 2009;80(20):205407.
[58] Sadd MH. Elasticity: theory, applications, and numerics. 2nd ed. Amsterdam: Boston Elsevier/AP; 2009.
[59] Tsai DH. The virial theorem and stress calculation in molecular dynamics. J Chem Phys 1979;70(03):1375–82.
[60] Zimmerman JA, Webb EBI, Hoyt JJ, Jones RE, Klein PA, Bammann DJ. Calculation of stress in atomistic simulation. Modell Simul Mater Sci Eng 2004;12:S319–32.
[61] Huang Y, Wu J, Hwang KC. Thickness of graphene and single-wall carbon nanotubes. Phys Rev B 2006;74(24):245413.
[62] Sakhaee-Pour A. Elastic properties of single-layered graphene sheet. Solid State Commun 2009;149:91–5.
[63] Scarpa F, Adhikari S, Srikantha Phani A. Effective elastic mechanical properties of single layer graphene sheets. Nanotechnology 2009;20:065709.
[64] Kudin KN, Scuseria GE, Yakobson BI. C2F, BN, and C nanoshell elasticity from ab initio computations. Phys Rev B 2001;64(23):235406.
[65] Arroyo M, Belytschko T. Finite crystal elasticity of carbon nanotubes based on the exponential Cauchy-Born rule. Phys Rev B 2004;69(11):115415.
[66] Liu F, Ming PM, Li J. Ab initio calculation of ideal strength and phonon instability of graphene under tension. Phys Rev B 2007;76(6):064120.
[67] Grantab R, Shenoy VB, Ruoff RS. Anomalous strength characteristics of tilt grain boundaries in graphene. Science 2010;330(6006):946–8.
[68] Lee C, Wei X, Kysar J, Hone J. Measurement of the elastic properties and intrinsic strength of monolayer graphene. Science 2008;321:385–8.
[69] Stoller MD, Park SJ, Zhu YW, An JH, Ruoff RS. Graphene-based ultracapacitors. Nano Lett 2008;8(10):3498–502.
[70] Stankovich S, Dikin DA, Dommett GHB, Kohlhaas KM, Zimney EJ, Stach EA, et al. Graphene-based composite materials. Nature 2006;442(7100):282–6.
[71] Kim EA, Neto AHC. Graphene as an electronic membrane. Eur Phys Lett 2008;84(5):57007.
[72] Sen D, Novoselov KS, Reis PM, Buehler MJ. Tearing graphene sheets from adhesive substrates produces tapered nanoribbons. Small 2010;6(10):1108–16.
[73] Lu Q, Arroyo M, Huang R. Elastic bending modulus of monolayer graphene. J Phys D-Appl Phys 2009;42(10):102002.
[74] Landau LD, Lifshitz EM, Kosevich AM, Pitaevskii LP. Theory of elasticity, course of theoretical physics. 3rd English ed. New York: Pergamon Press; 1986.
[75] Furukawa S, Uji-i H, Tahara K, Ichikawa T, Sonoda M, De Schryver FC, et al. Molecular geometry directed Kagome and honeycomb networks: toward two-dimensional crystal engineering. J Am Chem Soc 2006;128(11):3502–3.
[76] Humphrey W, Dalke A, Schulten K. VMD: Visual molecular dynamics. J Mol Graph 1996;14(33):33–8.